

Senior Design Final Report

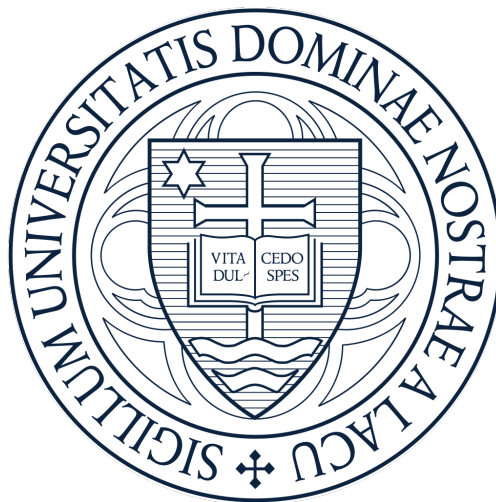
Department of Aerospace and Mechanical Engineering
University of Notre Dame

Prepared by: Greg Golonka, Anna Holloway, Ximena Romo,
Mike Scanlon, John Tuma, Timothy Welch

Prepared for: AME 40461 - Aerospace Design I
Stanislav Gordeyev

Notre Dame, Indiana 46556

December 19, 2024



Contents

1	Introduction	2
2	Conceptual Design	2
2.1	Mission Statement	2
2.2	Design Drivers	2
2.3	Design Choices and Concept Selection Process	4
2.4	Initial Performance Estimates	9
3	Preliminary Design	10
3.1	Wing Design	10
3.2	Fuselage Design	14
3.3	Tail Design	16
3.4	Control Surfaces Design	17
4	Manufacture Plan	20
4.1	Construction Plan	20
4.2	Material Consideration	24
4.3	Manufacturing Processes	24
5	Aircraft Performance Predictions	25
5.1	Lift and Drag Analysis	25
5.2	Stability Analysis	27
5.3	Take-off Velocity	29
5.4	Take-Off Distance	30
5.5	Cruise Speed	31
5.6	Loading	31
5.7	Turning	32
6	Aircraft Design Summary	33
6.1	Main Characteristics	33
6.2	Uniqueness	37

1 Introduction

Senior design for aerospace engineers spans two semesters at the University of Notre Dame. In the first semester's class, AME 40461, teams learn the theory behind aircraft design and subsequently use that theory to complete the conceptual and preliminary designs of their aircraft. Additionally, they make decisions concerning the manufacture plan for the aircraft, and provide predictions for the aircraft's ultimate performance in the Spring.

This report summarized and details the steps, decisions, and results of that process for senior design team 10: Please Neglect Air Resistance.

2 Conceptual Design

2.1 Mission Statement

The mission provided in the class AME 40461 was to design one plane for two types of flight: unloaded and loaded. Between these two flights, the parameters of payload weight, take-off distance, speed, cost, and uniqueness were to be optimized. As such the team generated the following mission statement to guide the subsequent senior design.

Utilize our knowledge of aerodynamics, structures, and materials to design, build, and fly a radio-controlled airplane to complete the particular mission of loaded and unloaded flight and maximize total score by considering payload, take-off distance, speed, cost, and uniqueness.

2.2 Design Drivers

2.2.1 Design Driver Formulation

Design drivers were generated through a combination of the general suggested mission requirements from T. C. Corke's *Design of Aircraft* [1] and the provided design score equations which will ultimately be used to evaluate the aircraft. Those equations are broken down into flight score, cost score, and uniqueness score. The flight score equation is

$$S_{flight} = \frac{1000}{(t_1 - 18.4)^{1.2}} + \frac{1000}{(d_1 + 8.76)^{1.7}} + \frac{1002}{t_2} + \frac{300}{(d_2 + 7.93)^{1.2}} + 50 \cdot F(N) \quad (1)$$

where t_1 , d_1 , t_2 , and d_2 are the times and take-off distances of the the unloaded and loaded flights, respectively, N is the number of golf balls carried in loaded flight and $F(N)$ is given by

$$F(N) = \frac{1}{2} \left(1 + erf \left(\frac{\ln(N) - \ln(12)}{0.75 \cdot \sqrt{2}} \right) \right) \quad (2)$$

The cost equation is

$$S_{cost} = 1 - erf \left(\frac{\$ - 250}{35.54\sqrt{2.4}} \right) \quad (3)$$

where $\$$ is the amount of money spent in USD. Finally, the uniqueness score is calculated via

$$S_{unique} = \frac{Points}{5} \quad (4)$$

where $Points$ is the average evaluation of the aircraft's uniqueness on a scale of 0-10.

As such, by combining these sources of information, the design drivers were determined to be:

- Maximized Golf Balls Carried
- Maximize Uniqueness
- Minimize Take-Off Distance
- Maximize Durability
- Minimize Cost
- Maximize Ease of Manufacture
- Maximize Speed
- Minimize Bank Radius

2.2.2 Design Driver Optimization

A MATLAB script was written to optimize the design drivers based on the flight score equations given in Equations 1-4. The purpose of the script was to determine the number of golf balls that would most likely optimized flight score, S_{flight} , since it was decided that S_{cost} and S_{unique} could be optimized independently of the flight score. This optimization relied on the assumption that take-off distance and flight time for both loaded and unloaded flight would increase with the number of golf balls carried in loaded flight. That relationship was represented by a proportionality, and the coefficients of proportionality were found by investigating the videos provided in the mission announcement. The result of this analysis was that the optimal number of golf balls was 35, which became the target payload for the group.

Furthermore, the fact that this neared the median number of golf balls for the historical data convinced the group that it should not focus on any one performance characteristic of aircraft too much, at the expense of others. As such, it was decided that a general plane with robust “all-around” performance would be designed.

2.2.3 Design Driver Weighting

For use in trade studies, the design drivers were weighted to reflect this decision to build a general performance plane. The weights of the design drivers are tabulated in Table 1.

Table 1: Design driver weights.

Figures of Merit	Quantitative Weight
Number of golf balls	16
Uniqueness	10
Take-Off Distance	13
Durability	8
Cost	13
Ease of Manufacture	20
Speed	15
Bank Radius (min)	5

2.3 Design Choices and Concept Selection Process

2.3.1 Wing Mounting

The first concept selection trade study was performed on the wing mounting. Three options were considered:

- High Wing
- Low Wing
- Mid Wing

These were chosen as a result of the team's initial brainstorming phase. The design concepts were evaluated against the design drivers summarized in Table 1. The result of this trade study was that the high wing mounting was chosen due to the increased stability and carry weight that it would provide. That decision was made using theoretical understanding gained from Flight Dynamics. The complete ranking of designs in the trade study along with the final result are summarized in Table 2.

Table 2: Wing mounting trade study.

Figures of Merit	Weight (%)	High Wing	Low Wing	Mid Wing
				
Number of golf balls	16	5.0	1.0	3.0
Uniqueness	10	3.0	3.0	3.0
Take-Off Distance	13	4.0	3.5	3.0
Durability	8	3.5	3.0	4.0
Cost	13	3.0	3.0	3.0
Ease of Manufacture	20	3.0	3.0	3.0
Speed	15	2.0	5.0	3.0
Bank Radius (min)	5	1.0	5.0	3.0
Total	100	3.24	3.15	3.08

2.3.2 Wing Configuration

A concept selection trade study was also performed on the wing configuration. Four options were considered:

- Anhedral
- Dihedral
- Gull Wing
- Straight Wing

These were chosen as a result of the team's initial brainstorming phase. These design concept were also evaluated against the design drivers summarized in Table 1.

The initial result of this trade study was that the wing anhedral was chosen prior to the conceptual design review. It was chosen due to the increased uniqueness. However, the team was aware of the decreases in performance and ease of manufacturability. As such, after receiving feedback from the conceptual design review, the team re-evaluated this trade study and instead chose the straight wing design for its optimal performance and ease of manufacturability. The complete ranking of designs in the trade study along with the final result are summarized in Table 3.

Table 3: Wing configuration trade study.

Figures of Merit	Weight (%)	Anhedral	Dihedral	Gull Wing	Straight Wing
Number of golf balls	16	4.0	3.0	4.0	5.0
Uniqueness	10	4.5	3.0	5.0	1.0
Take-Off Distance	13	3.0	3.5	4.0	3.0
Durability	8	4.0	4.0	2.0	4.0
Cost	13	3.5	3.5	2.0	4.0
Ease of Manufacture	20	3.5	3.5	1.0	5.0
Speed	15	3.0	5.0	3.0	3.0
Bank Radius (min)	5	5.0	4.0	2.0	2.5
Total	100	3.66	3.66	2.83	3.71

2.3.3 Wing Shape

The concept selection trade study performed on the wing shape considered four options:

- Rectangular
- Trapezoidal (Tapered, Unswept)
- Elliptical
- Swept Wing

Senior Design Final Report

These were chosen as a result of the team's initial brainstorming phase. These design concepts were also evaluated against the design drivers summarized in Table 1. The result of this trade study was the selection of the trapezoidal wing. It was chosen for its superior performance compared to a rectangular wing, but also its greater ease of manufacturing compared to an elliptical wing. The complete ranking of designs in the trade study along with the final result are summarized in Table 4.

Table 4: Wing shape trade study.

					
Figures of Merit	Weight (%)	Rectangular	Trapezoidal	Elliptical	Swept Wing
Uniqueness	12	1.0	4.0	5.0	5.0
Take-Off Distance	20	4.0	3.5	4.0	3.0
Durability	15	4.0	4.0	3.0	4.0
Cost	13	4.0	3.5	3.0	4.0
Ease of Manufacture	20	5.0	4.0	1.0	2.0
Speed	15	3.5	5.0	4.5	5.0
Bank Radius (min)	5	3.0	4.0	2.5	3.0
Total	100	3.72	3.99	3.24	3.62

2.3.4 Wing Airfoil

The concept selection trade study performed on the wing shape considered four options:

- Clark Y
- NACA 2213
- N-22
- SD7037

These were chosen as a result of the team's initial research into common airfoils for RC planes and gliders [2],[3],[4],[5]. Because the selection of airfoils applies itself to more specific design criteria than those summarized in Table 1, these airfoils were compared against additional metrics of their aerodynamic performances, as obtained in XFLR5 [6]. The result of this analysis was that the N-22 airfoil was chosen for its superior lift and ease of manufacture. The complete ranking of designs in the trade study along with the final result are summarized in Table 5.

Table 5: Wing airfoil trade study.

Figures of Merit	Weight (%)	Clark Y	NACA 2213	N-22	SD7037
Uniqueness	10	3.0	4.0	3.0	5.0
Ease of Manufacture	20	5.0	3.0	5.0	2.0
C_l , max	14	1.2	1.0	1.5	1.3
C_d at C_l , max	14	1.2	1.1	1.5	1.2
C_{lo}	14	0.1	0.7	3.0	1.2
C_{do}	14	1.2	1.2	1.5	1.0
Max L/D	14	1.3	1.1	1.3	1.3
Total	100	2.0	1.7	2.5	1.7

2.3.5 Fuselage Shape

The concept selection for the fuselage shape considered three options:

- Rectangular body with a flat face
- Rectangular body with a nose cone
- Cylindrical body with and inverted camber

These three options were tested using SolidWorks flow simulations to determine which would be the most aerodynamically efficient, while also maintaining manufacturability. The result was that the rectangular body with nose cone was selected for its low drag and easy manufacturing. The exact flow simulations performed are discussed further in Section 3.

2.3.6 Tail Configuration

The concept selection trade study performed on the tail configuration considered five options:

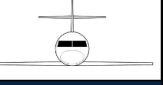
- V-Tail
- Cruciform
- Conventional
- T-Tail
- H-Tail

These were chosen as a result of the team's initial brainstorming phase. These design concept were also evaluated against the design drivers summarized in Table 1. The result of this trade study was the selection of the conventional tail. It was chosen for its superior performance and greater ease of manufacturing. However, the team did seek feedback on the tail selection because research showed that planes with a high wing configuration benefited from having a T-tail [7]. However, feedback during the conceptual design review informed that team that for planes as small as RC planes, the T-tail would provide no improved performance.

Senior Design Final Report

As such, the team decided to continue with its design of a conventional tail. The complete ranking of designs in the trade study along with the final result are summarized in Table 6.

Table 6: Tail configuration trade study.

						
Figures of Merit	Weight (%)	V Tail	Cruciform	Conventional	T Tail	H Tail
Number of golf balls	16	1	2	4	5	3
Uniqueness	10	4	2	1	3	5
Take-Off Distance	13	3	4	5	2	1
Durability	8	1	2	5	3	4
Cost	13	5	2	4	3	1
Ease of Manufacture	20	2	3	4	5	1
Speed	15	5	3	4	2	1
Bank Radius (min)	5	4	3	5	2	1
Total	100	3.03	2.66	3.96	3.39	1.96

It is worth noting that, after the conceptual design phase, the team decided to add a small, single boom tail to the design. This was done to improve uniqueness and longitudinal stability without sacrificing much ease of manufacturing. This decision was informed by the theory learned in Flight Dynamics.

2.3.7 Tail Airfoils

The tail airfoil was selected based on multiple necessary characteristics of rudder and elevator design. Of greatest importance was that the airfoil be symmetric in order to produce equal force on both sides of the wing and minimal drag at no angle of attack. Therefore, the symmetric foil also promotes directional and longitudinal stability and reduces the hinge moment of the rudder and elevator flaps. It was deemed that the NACA airfoil database would be our best resource for symmetric airfoils, and the NACA 0010 offers optimal mission capability due to its high lift potential and minimal drag profile. For visual aid, the shape of the NACA 0010 airfoil is included in Figure 1.



Figure 1: NACA 0010 Airfoil

2.3.8 Landing Gear Configuration

The concept selection performed on the landing gear configuration did not include a trade study as the design concepts selected previously limited the possible tail configuration to one option. This is because the choice of high wings precluded any form of outrigger wheels. Furthermore, the length of the fuselage would make the implementation of tricycle landing gear complicated. As such, the taildragger configuration of landing gear was selected. An example of this landing gear configuration, for visual aid, is shown in Figure 2.



Figure 2: Example of taildragger configuration of landing gear.

2.4 Initial Performance Estimates

2.4.1 Weight Estimates

Since an accurate weight estimate would not be possible until a high-fidelity mock-up of the aircraft, with complete components list was created, preliminary weight estimates were found for the initial analysis. These estimates were found using the historical data for the last two classes of senior design. Specifically, across all the planes created in the past two years, the average unloaded and loaded weights per golf ball carried in loaded flight were calculated to be 0.242 lbf and 0.344 lbf, respectively. Multiplying these values by the target number of golf balls, 35, yielded estimated unloaded and loaded weights of $W_{unloaded} = 8.487$ lbf and $W_{loaded} = 12.031$ lbf.

2.4.2 Thrust Estimates

To estimate the thrust produced by the propulsion system, a methodical approach was followed involving the propeller and motor provided. A Master Airscrew 12x6 propeller was provided as part of the givens for the thrust generation. The propulsion system employs a single puller motor configuration, simplifying the design and ensuring adequate power delivery while maintaining a favorable thrust-to-weight ratio. This motor configuration also increases the stability, efficiency, and manufacturability of the aircraft. The motor provided is the E-Flite Power 46 to drive the propeller.



Figure 3: Provided propeller and motor components.

Using Actuator Disk Theory for the static case ($V_\infty = 0$), the theoretical thrust was estimated. The calculation used the following parameters: engine power ($P_{engine} = 0.53$ hp), density of air at sea level ($\rho = 0.0023$ slug/ft³) and the area of the disc ($A_{disc} = 0.78$ ft²). The theoretical static thrust T_0 was computed as:

$$T_0 = P_{engine}^{2/3} (2\rho A_{disc})^{1/3} \quad (5)$$

The resulting theoretical thrust was found to be $T_{theoretical} = 7.6$ lbf. It is important to emphasize that this thrust value is only a preliminary estimate based on theoretical calculations and ideal conditions. Actuator Disk Theory doesn't account for real world effects such as blade tip losses, non-uniform flow, or wake rotation. Actual thrust data will be acquired next semester during real propulsion testing, once the selected motor, propeller, and associated components are available. These tests will provide a more accurate assessment of the system's performance under realistic operating conditions.

3 Preliminary Design

3.1 Wing Design

3.1.1 Geometry and Aerodynamics

Based on the concept selection made in the conceptual design phase, geometric parameters defining the plane's wings were chosen. These parameters are summarized in Table 7.

Table 7: Geometric wing parameters.

Geometric Parameters	
Parameter	Value
Airfoil	N-22
Area, S	816.66 in ²
Span, b	70 in.
Aspect Ratio, AR	6.0
Root Chord, c_r	16.66 in.
Tip Chord, c_t	6.66 in.
Taper Ratio, λ	0.4
Oswald's Efficiency, ϵ	0.8691
MAC, \bar{c}	12.38 in.
LE Sweep, Λ_{LE}	4.336°
$\bar{c}/4$ Sweep, $\Lambda_{\bar{c}/4}$	0°
$\bar{c}/4$ Thickness, $(t/\bar{c})_{\bar{c}/4}$	12.215%
Max Thickness, $(t/\bar{c})_{max}$	12.4%

The parameters allowed for the wing to be fully defined and for an initial XFLR5 study to be conducted. The purpose of this study was to acquire preliminary values on lift and drag

for the wing which could be used to calculate speeds and loads needed for the remainder of the wing design. Many of these values changed later as the full-plane was designed, and those final values are listed in Section 5. Basic results of the XFLR5 study are shown in Figure 4.

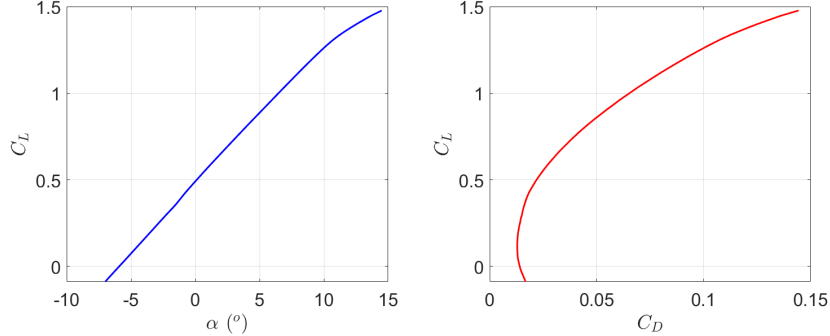


Figure 4: Plots of C_L vs. α and C_L vs C_D .

Those aerodynamics parameters which were calculated based on the data from the initial XFLR5 study are tabulated in Table 8.

Table 8: Aerodynamic wing parameters.

<u>Initial Aerodynamic Parameters</u>	
Parameter	Value
C_{L0}	0.49
$(C_{L\alpha})$	4.584 /rad
C_{Lmax}	1.48
C_{D0w}	0.043
Stall Speed, v_s	30.1 ft/s
Cruise Speed, v_c	50.7 ft/s
Dive Speed, v_d	76.05 ft/s

3.1.2 Rib and Spar Design

Those aerodynamic parameters allowed for a loading analysis to be conducted using the theory learned in Aerospace Structures. A program was written in MATLAB to conduct this analysis, and it considered the load factors both in still air and gusts, which can be very significant in Spring in South Bend, especially relative to the size and weight of an RC plane. Figure 5 shows the n-v envelope, or flight envelope, for the proposed plane. It incorporates three different magnitudes of gusts, prescribed in Megson's textbook, Aircraft Structures for Engineering Students [8].

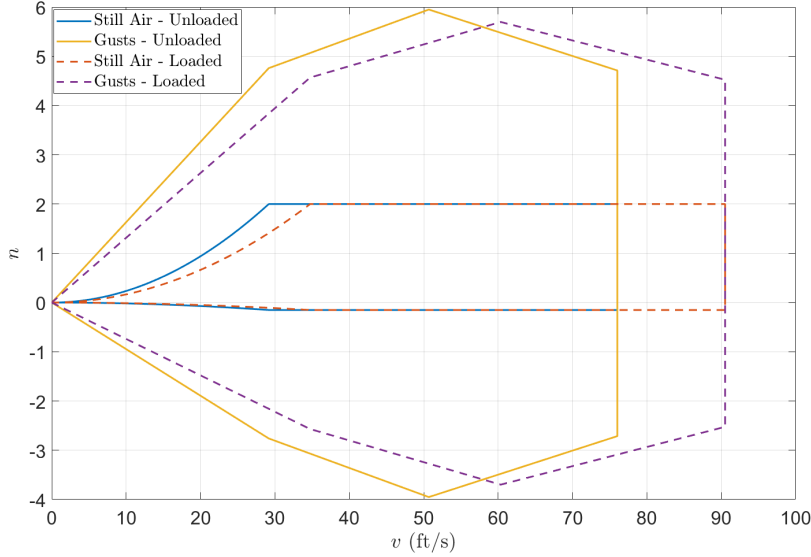


Figure 5: Flight envelope for still-air and gusty flight.

The significant results of that plot are also summarized in Table 9. The most severe load factor drives the design, which was a load factor experienced under gusts of $n = 5.95$. This value appears to be higher than typical values for full-sized aircraft, given the relatively high magnitude of wind gusts to the airspeed of an RC craft, it is believed to be accurate. Additionally, it is similar to values found for other RC aircraft [9].

Table 9: Maximum load factors.

Max Loads	
Loading Condition	Value
Still Air - Unloaded	2.1
Gusts - Unloaded	5.95
Still Air - Loaded	2.1
Gusts - Loaded	5.70

This maximum load factor was used to calculate the number of ribs required for the wing, which will ultimately support the load of lift. A MATLAB script was used to perform this analysis, but the general process began by calculating the total force on one wing with the equation

$$\sum F = \frac{n_{max} W}{2} \quad (6)$$

where $\sum F$ is the total force on one wing, n_{max} is the maximum load factor of 5.95, and W is the loaded weight, which was used since it presents a more severe case than the unloaded weight.

The next step involved a solid mechanical analysis. As will be discussed in Section 4, the ribs are to be manufactured from 1/8th inch plywood, which had a rolling shear yield strength of 250 psi [10]. Assuming a Factor of Safety of 2 and that all the weight will be on the main spar, the force on each beam is given as

$$F = t \cdot b \cdot \tau_y \quad (7)$$

where t is the thickness of 1/8th inch, b is the minimum distance between the main spar and top of rib, which varies along the span, and τ_y is the post-Factor of Safety yield strength of 125 psi. The forces were distributed according to the lift distribution of the wing generated in the initial XFLR5 analysis, which is shown in Figure 6.

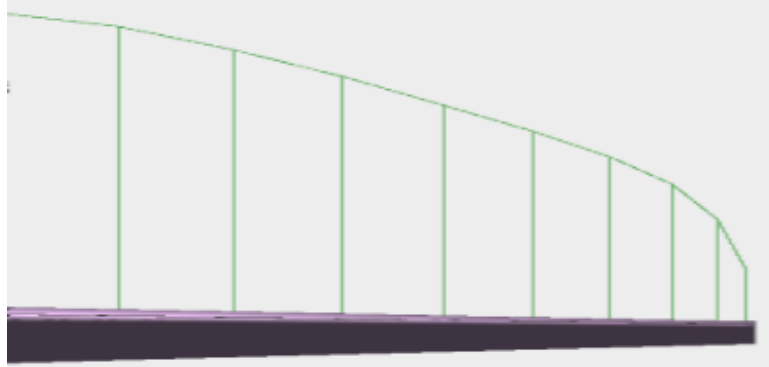


Figure 6: Lift distribution over half the wing from XFLR5.

The result of the MATLAB FEA analysis was that the wing should have 9 equally spaced ribs, arranged as shown in Figure 7.

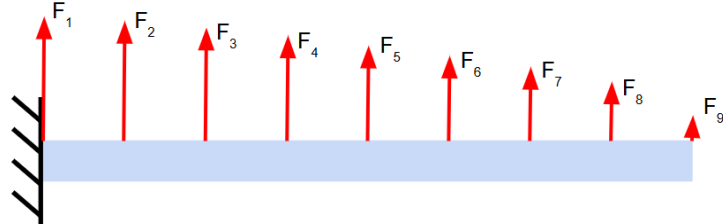


Figure 7: Force distribution on ribs over half the wing.

These ribs would each support a load less than their maximum load given by Eq 7. This is demonstrated graphically in Figure 8.

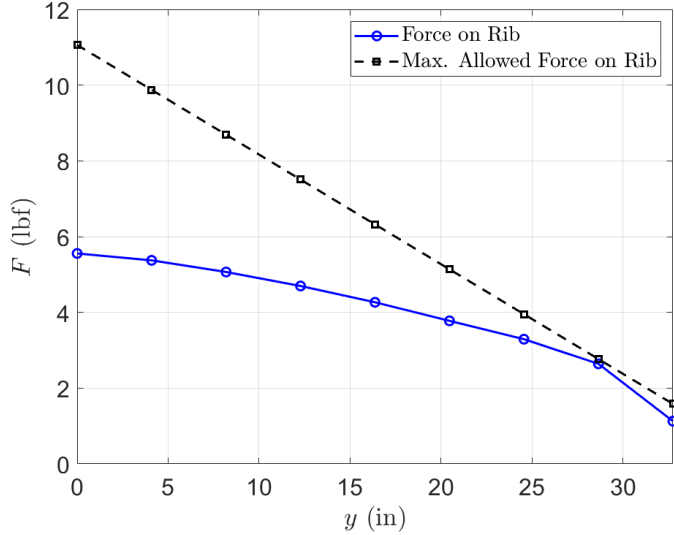


Figure 8: Calculated and maximum rib loading.

Finally, this analysis allowed for the creation of shear-moment diagrams on the wing, given that it is treated as a cantilever beam, which are shown in Figure 9.

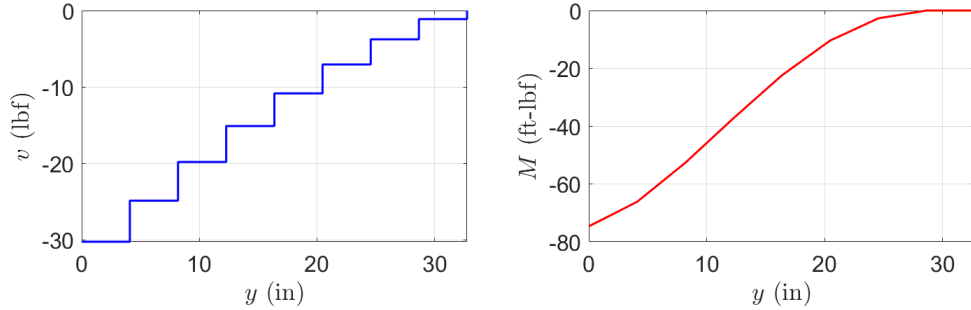


Figure 9: Shear moment diagrams for wing.

This concludes the analysis needed for the preliminary design of the wing. Further load analysis, including a discussion of the wing's maximum moment and shear loading and a SolidWorks FEA analysis of the main spar are included in Section 5.

3.2 Fuselage Design

Using the three initial fuselage designs outlined in Section 2.3.5, a drag simulation was conducted to compare each design. Additionally, the fuselage designs were compared by their ability to store both the payload and internal electrical components. To conduct the drag testing on the different fuselage designs, a rough model was made for each design in Solidworks for testing. Figure 10 shows the different Solidworks designs used for testing.

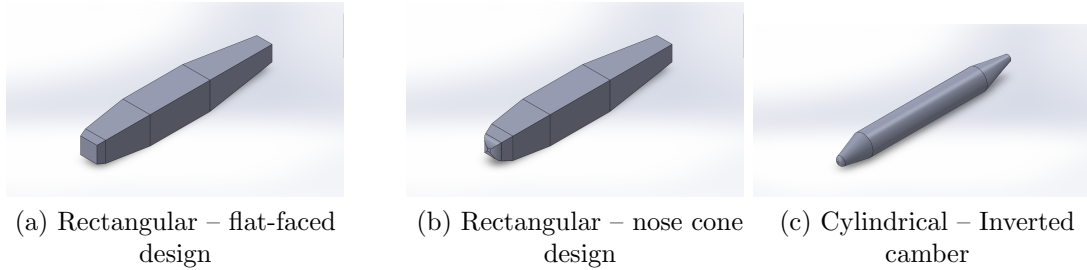


Figure 10: Fuselage conceptual designs

Flow simulations were then used to calculate the total drag on the different fuselage designs. The results of the initial testing can be found in Table 10.

Table 10: Initial results from Solidworks flow simulations

Fuselage Design	Drag	Units
Flat faced Design	0.173	N
Nose cone Design	0.041	N
Cylindrical Design	0.024	N

From the initial drag testing, the cylindrical design was proven to reduce the drag of the fuselage as predicted. However, the addition of a nose cone to the flat-faced rectangular design reduced the overall drag production to a negligible difference between the cylindrical design and the flat-faced design. The increased labor and difficulty needed to make a cylindrical design would have minimal design benefits compared to adding a nose cone.

The final geometry of the final fuselage design is a combination of the cylindrical and nose cone models. Ultimately, the size of the fuselage was calculated to hold the target 35 golf balls, and all internal components provided. The final fuselage design is shown in Figure 11,

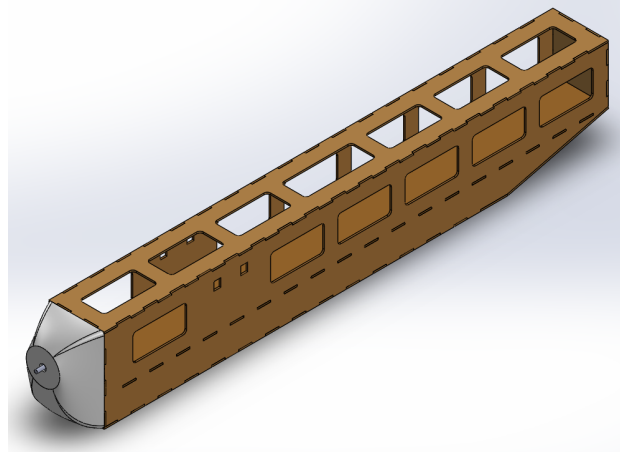


Figure 11: Final fuselage design

The final fuselage has cross-sectional dimensions of 4.125" x 6.25" with a length of 37.5", not including the nose cone. The main compartment of the fuselage is divided into upper and lower compartments for avionics and payload separation. The final fuselage design holds 348.75 in³. Additionally, the nose cone is designed to house the motor to further reduce drag.

Using a simplified assembly in Solidworks, the total drag and base drag coefficient were simulated while keeping the landing gear attached. The results of the flow simulations can be found in Figure 12.

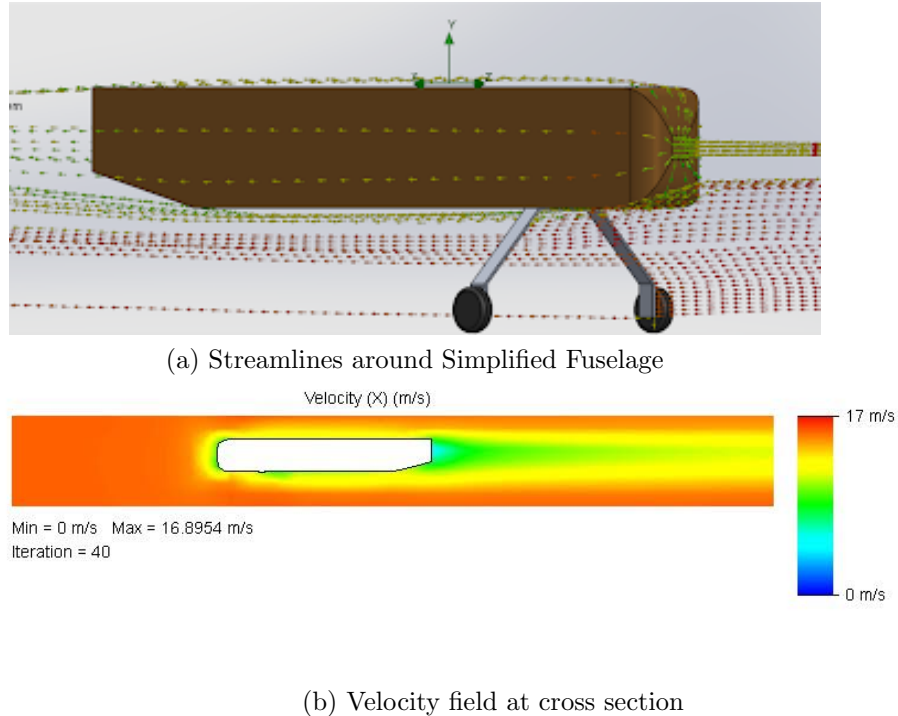


Figure 12: Solidworks flow simulations results

The results from the flow simulation can be found in Table 11,

Table 11: Final results from Solidworks flow simulations

Drag	C_{D0}
2.176 [N]	0.02537

3.3 Tail Design

3.3.1 Horizontal Tail Design

The size of the horizontal tail was calculated using a set of defined wing dimensions from the initial calculation of the wing size and using the historical value for the horizontal tail coefficient, $C_{HT} = 0.5$.

$$S_{HT} = C_{HT} \frac{(\bar{c}_W S_W)}{l_{HT}} \quad (8)$$

where $S_W = 816.67$ in and $\bar{c}_W = 12.38$ in. The length to the horizontal tail, l_{HT} was approximated to be 0.55 times the length of the aircraft, $L = 61.5$ in. From this approximation, $l_{HT} = 33.825$ in. The results of the calculation from Equation 8 produced tail sizing parameters of $S_{HT} = 149.45$ in². From historical data, the aspect ratio of the stabilizer, AR_{HT} , is taken to be 50% of the main wing aspect ratio and thus was calculated to be 3. A rectangular shape with no taper was chosen for ease of manufacturing.

3.3.2 Vertical Tail Design

Similar to the sizing process of the horizontal tail, the size of the vertical tail was calculated from main wing dimensions for the vertical tail coefficient, $C_{VT} = 0.04$.

$$S_{VT} = C_{VT} \frac{(\bar{c}_W S_W)}{l_{VT}} \quad (9)$$

The length to the vertical tail, l_{VT} assumed to be equal to l_{HT} . From this approximation, $l_{VT} = 33.825$ in. The results of the calculation from Equation 9 produced a vertical tail area of $S_{VT} = 67.6$ in². From historical data, the optimal aspect ratio of the vertical stabilizer, AR_{VT} , is 1.6. Again, a rectangular shape was chosen for manufacturing purposes.

3.4 Control Surfaces Design

3.4.1 Flaperon Design

The flaperons were initially sized using DBF historical guidelines. The area and span of the flaperons were calculated as 25% and 50% of the wing area and span, respectively, resulting in an area of $S_f = 204.167$ in², a span of $b_f = 35$ in, and from these values a chord of $c_f = 5.833$ in. To aid in the manufacturing of the wing such that the spars line up with the flaperon, the team modified these values resulting in an area of $S_f = 148.95$ in², a span of $b_f = 33.1$ in, and a chord of $c_f = 4.5$ in. The design of the flaperons can be seen in Figure 13.

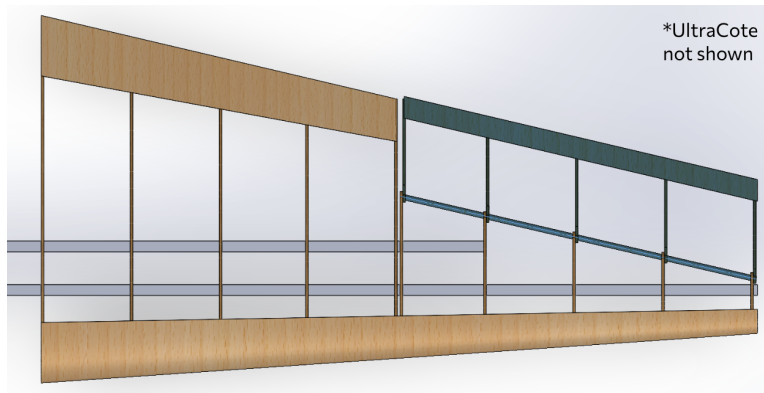


Figure 13: Flaperon design.

3.4.2 Elevator Design

The elevator flaps were sized following the methods taught in class in addition to DBF historical sizing for comparison. To size the elevator, the following equations were used:

$$\Delta C_m = (C_{m,\delta_e})\delta_e = -C_{m_0} - (C_{m,\alpha})\alpha, \quad (10)$$

$$(C_{m,\delta_e}) = \frac{\Delta C_m}{\delta_e}, \quad (11)$$

$$(C_{m,\delta_e}) = -V_H\eta\tau(C_{L,\alpha}), \rightarrow \tau = \frac{-(C_{m,\delta_e})}{V_H\eta(C_{L,\alpha})}. \quad (12)$$

Substituting in values gathered from XFLR5 and the previously calculated wing geometry, the flap effectiveness parameter for the elevator flaps was determined from Robert C. Nelson's textbook, Flight Stability and Automatic Control [11]. It was determined to be $\tau = 0.13$.

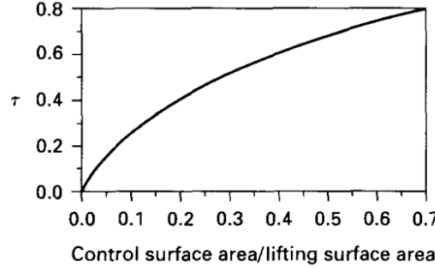


FIGURE 2.21
Flap effectiveness parameter.

Figure 14: Sizing chart for flap effectiveness parameter.

Utilizing the calculated flap effectiveness parameter with the sizing chart provided in Figure 14, it was determined that the elevator flaps should be 30% of the wing area with the same wing span, resulting in a calculated area of $S_e = 44.835 \text{ in}^2$. This aligns with the historical DBF sizing, which determined that the elevator flaps should be approximately 30% of the wing area. The elevator flap design is shown in Figure 15.

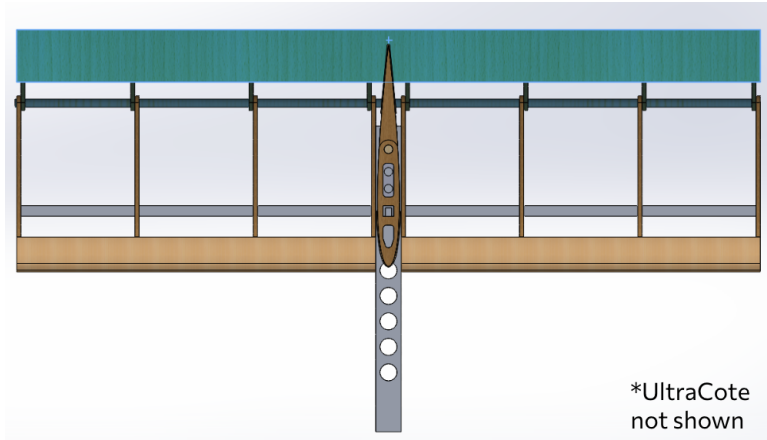


Figure 15: Elevator flap design.

3.4.3 Rudder Design

The rudder flap was sized in a similar manner to the elevator flaps, following both the method taught in class in addition to DBF historical sizing for comparison. To size the rudder, the following equations were used:

$$\Delta C_m = (C_{m,\delta_r})\delta_r = -C_{m_0} - (C_{m,\alpha})\alpha, \quad (13)$$

$$(C_{m,\delta_r}) = \frac{\Delta C_m}{\delta_r}, \quad (14)$$

$$(C_{m,\delta_r}) = -V_V\eta\tau(C_{L,\alpha}), \rightarrow \tau = \frac{-(C_{m,\delta_r})}{V_V\eta(C_{L,\alpha})}. \quad (15)$$

These are the same equations, modified to use values from the rudder and vertical tail rather than the elevator and horizontal tail. Likewise, the flap effectiveness parameter was calculated to be $\tau = 0.287$, and from Figure 14, this resulted in a rudder flap with 47% of the vertical tail area, $S_r = 31.772 \text{ in}^2$. This was slightly smaller than the DBF historical sizing, which, like the elevator, sized the rudder to also be 30% of the horizontal tail area. This would have resulted in a rudder area of $S_r = 44.835 \text{ in}^2$. The team decided to go with the calculation based on the vertical tail rather than the horizontal tail, and the design of the rudder can be found in Figure 16 below.

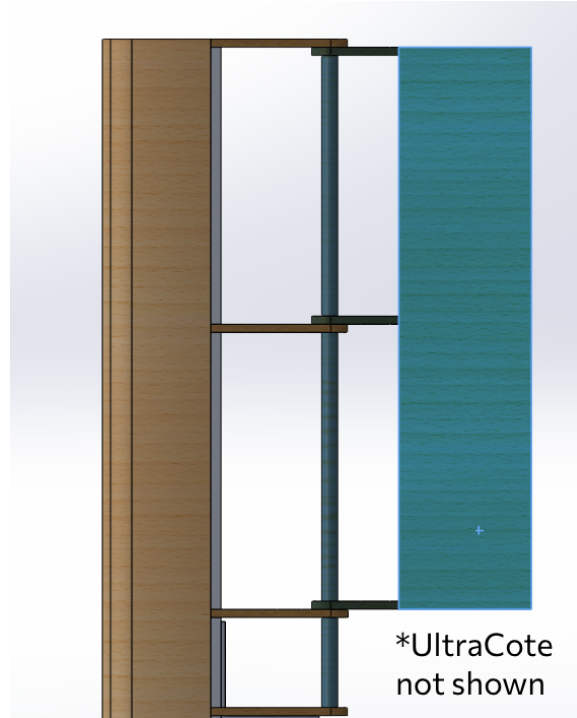


Figure 16: Rudder flap design.

4 Manufacture Plan

4.1 Construction Plan

4.1.1 Wings and Tails

The two material options for the construction of the wings were wood and aluminum or wire-cut foam. These were the two options considered because they allowed for the manufacture of the desired shapes while still minimizing weight. It was ultimately decided to create the wings out of a wood-aluminum structure as this afforded the team a greater ability to address stress, loading, and geometry concerns than a single piece of foam would.

The plan for these structures is to run spars through ribs, cut to match the desire airfoil shape. For the wing, these spars will run through the fuselage, eliminating the need for a wing-box. For the horizontal tail, this spar will run through the boom. The spar for the vertical tail will simply attach to the boom via an L-Bracket.

Thin sheeting will also be used on the leading and trailing edges of the wings and tails. The purpose of this sheeting is to provide structure and to allow the UltraCote, which will be used to wrap the structure, to adhere to the wings and tail respectively.

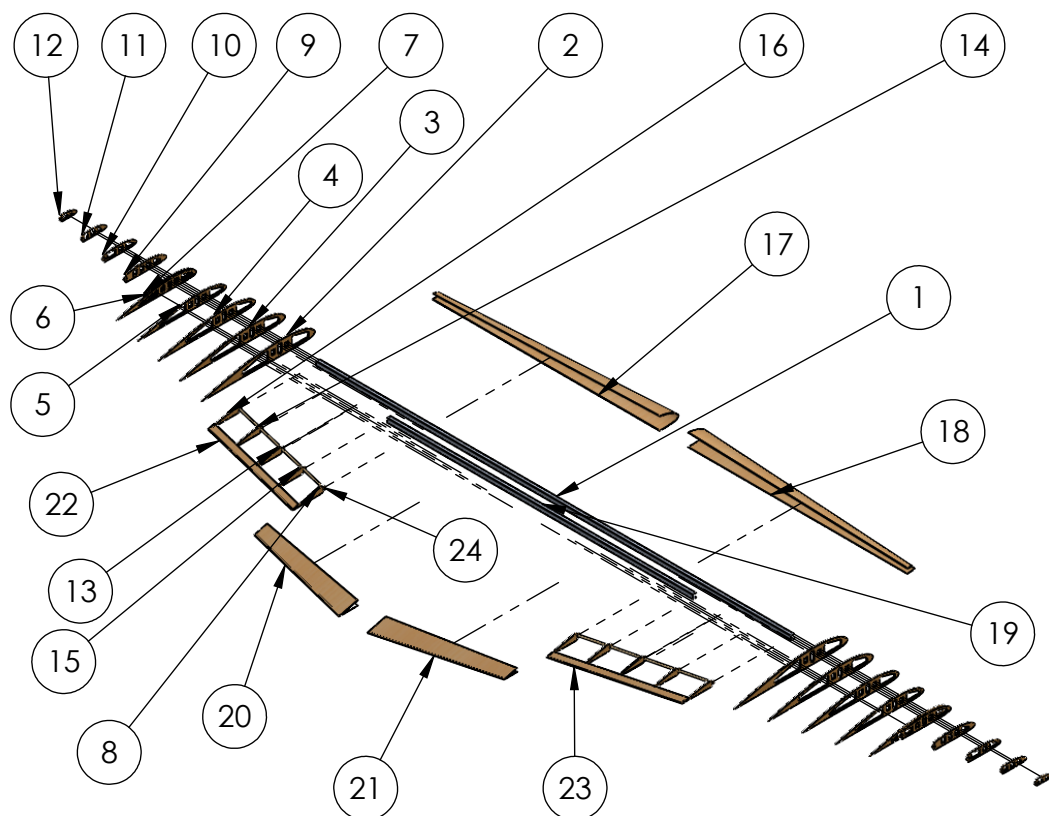
The ribs used for the control surfaces will be split into rib sections for the main wing/tail and rib sections for the control surface. These sections will be connected via a dowel rod [12] and will be actuated by servos.

Finally, the boom [13] connecting the tail to the fuselage will be purchased cheaply, cut to size, and drilled with speed holes to reduce weight.

4.1.2 Fuselage

The fuselage will be constructed out of panels which will be constructed in a "jigsaw" fashion and held firm with glue. The boom shall be connected to the fuselage via an L-bracket. The nose cone and motor will be connected through basic fasteners to the front plate of the fuselage. The landing gear, which will be purchased will also be attached via basic fasteners to the bottom plate of the fuselage.

Engineering drawings detailing this manufacture plan via orthographic exploded views are included subsequently.



ITEM NO.	PART NUMBER	QTY.
1	wingSparOption1	1
2	wingRib1	2
3	wingRib2	2
4	wingRib3	2
5	wingRib4	2
6	wingRib5	2
7	wingRib5Split	2
8	wingRib5Aileron	2
9	wingRib6Split	2
10	wingRib7Split	2
11	wingRib8Split	2
12	wingRib9Split	2
13	wingRib7Aileron	2
14	wingRib8Aileron	2
15	wingRib6Aileron	2
16	wingRib9Aileron	2
17	wingLESheeting	2
19	wingSparSecondaryOption1	1
20	wingTESheeting	2
22	wingAileronSheeting	2
24	aileronRod	2



PROPRIETARY AND CONFIDENTIAL
THE INFORMATION CONTAINED IN THIS DRAWING IS THE SOLE PROPERTY OF NOTRE DAME ENGINEERING. ANY REPRODUCTION IN PART OR AS A WHOLE WITHOUT THE WRITTEN PERMISSION OF NOTRE DAME ENGINEERING IS PROHIBITED.

UNLESS OTHERWISE SPECIFIED:
DIMENSIONS ARE IN INCHES
TOLERANCES:
ANGULAR: MACH $\pm 1^\circ$
ONE PLACE DECIMAL ± 0.2
TWO PLACE DECIMAL ± 0.01
THREE PLACE DECIMAL ± 0.005
INTERPRET GEOMETRIC
TOLERANCING PER: ASME Y14.5

MATERIAL

FINISH

DO NOT SCALE DRAWING

NEXT ASSY
USED ON
APPLICATION

NAME DATE
DRAWN
CHECKED
ENG APPR.
MFG APPR.
Q.A.
COMMENTS:

ND ENGINEERING

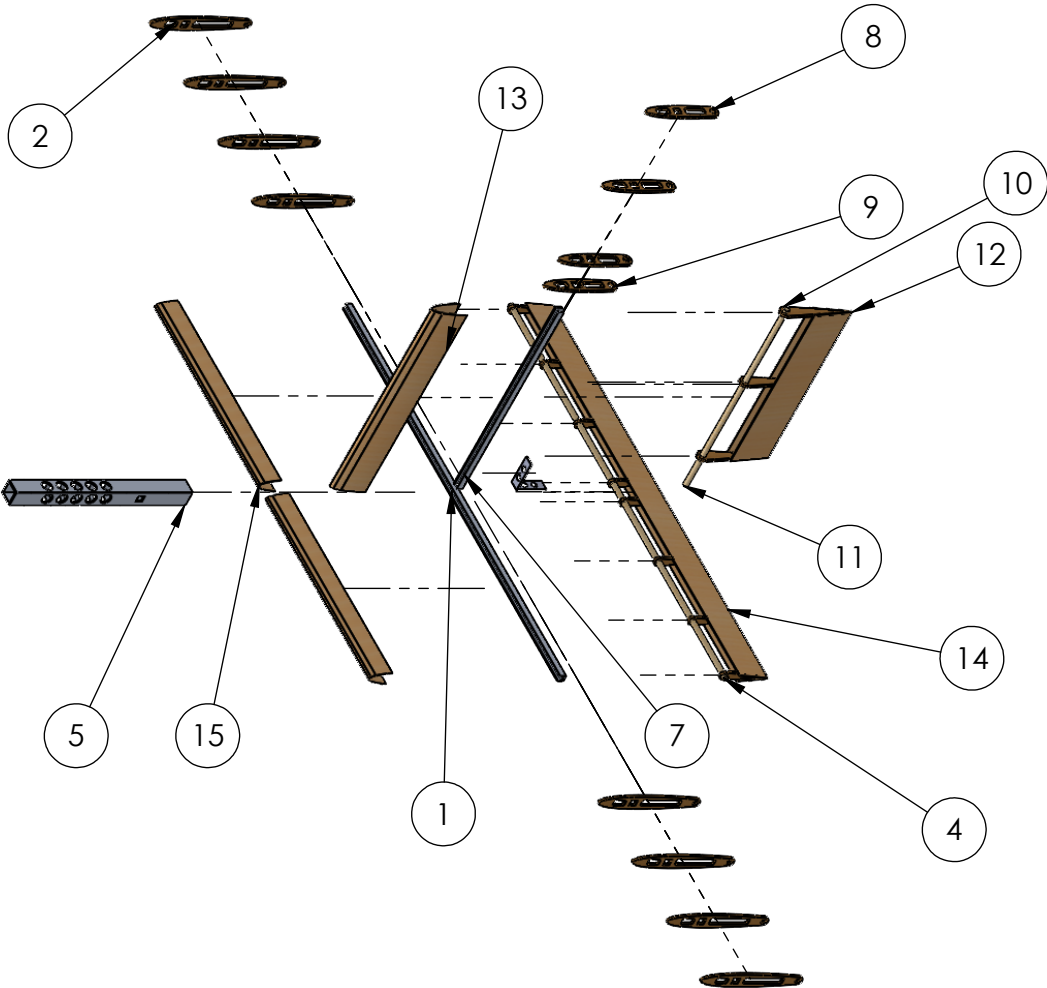
TITLE:

Wings - Exploded

SIZE	DWG. NO.	REV
A	WINGS-2	
SCALE: 1:48		SHEET 1 OF 1

2

1



ITEM NO.	PART NUMBER	QTY.
1	9001K747	1
2	HTLRibSplit	8
3	HTLRibElevator	8
4	elevatorRod	1
5	boom	1
6	VTBracket	1
7	9001K747	1
8	VTRibSplit	3
9	VTRibSplitRoot	1
10	VTRibRudder	3
11	rudderRod	1
12	rudderSheeting	1
13	VTLESheeting	1
14	elevatorSheeting	1
15	HTLESheeting	2



PROPRIETARY AND CONFIDENTIAL
THE INFORMATION CONTAINED IN THIS DRAWING IS THE SOLE PROPERTY OF NOTRE DAME ENGINEERING. ANY REPRODUCTION IN PART OR AS A WHOLE WITHOUT THE WRITTEN PERMISSION OF NOTRE DAME ENGINEERING IS PROHIBITED.

UNLESS OTHERWISE SPECIFIED:	NAME	DATE
DIMENSIONS ARE IN INCHES	DRAWN	
TOLERANCES:	CHECKED	
ANGULAR: MACH $\pm 1^\circ$	ENG APPR.	
ONE PLACE DECIMAL ± 0.2	MFG APPR.	
TWO PLACE DECIMAL ± 0.01	Q.A.	
THREE PLACE DECIMAL ± 0.005	COMMENTS:	
INTERPRET GEOMETRIC TOLERANCING PER: ASME Y14.5		
MATERIAL		
NEXT ASSY	USED ON	FINISH
APPLICATION	DO NOT SCALE DRAWING	

ND ENGINEERING

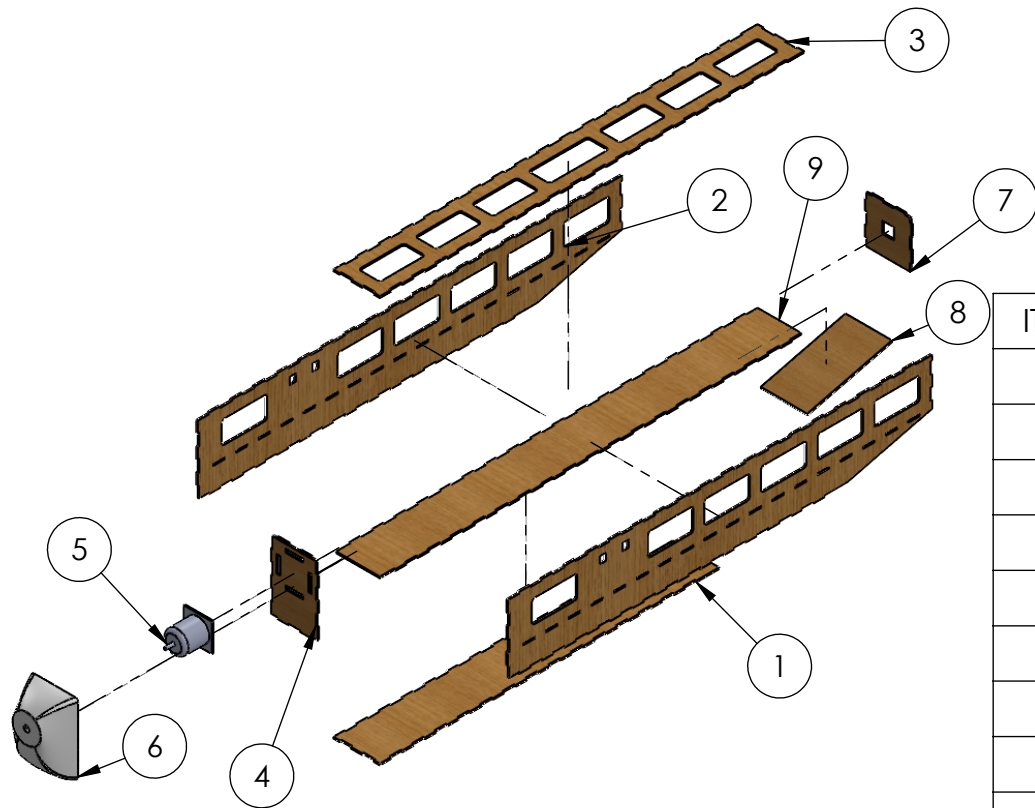
TITLE:

Tail-Exploded

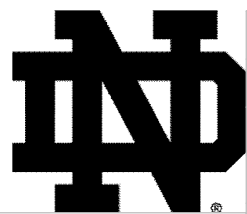
SIZE	DWG. NO.	REV
A	TAIL-2	
SCALE: 1:24		SHEET 1 OF 1

2

1



ITEM NO.	PART NUMBER	QTY.
1	fuselageBottom	1
2	fuselageSide	2
3	fuselageTop	1
4	fuselageFront	1
5	EFliteMotorLowFidel	1
6	noseCone	1
7	fuselageBack	1
8	fuselageHatch	1
9	fuselageMiddle	1



PROPRIETARY AND CONFIDENTIAL
THE INFORMATION CONTAINED IN THIS DRAWING IS THE SOLE PROPERTY OF NOTRE DAME ENGINEERING. ANY REPRODUCTION IN PART OR AS A WHOLE WITHOUT THE WRITTEN PERMISSION OF NOTRE DAME ENGINEERING IS PROHIBITED.

UNLESS OTHERWISE SPECIFIED:
DIMENSIONS ARE IN INCHES
TOLERANCES:
ANGULAR: MACH $\pm 1^\circ$
ONE PLACE DECIMAL ± 0.2
TWO PLACE DECIMAL ± 0.01
THREE PLACE DECIMAL ± 0.005

INTERPRET GEOMETRIC
TOLERANCING PER: ASME Y14.5

MATERIAL

NEXT ASSY USED ON

APPLICATION

FINISH

DO NOT SCALE DRAWING

NAME DATE

DRAWN

CHECKED

ENG APPR.

MFG APPR.

Q.A.

ND ENGINEERING

TITLE:

Fuselage Exploded

SIZE	DWG. NO.	REV
A	FUSELAGE-2	
SCALE: 1:32		SHEET 1 OF 1

4.2 Material Consideration

4.2.1 Plywood

1/8th inch plywood will be used for the wing and tail ribs and for the fuselage panels. It was selected due to its light weight, low cost, and reasonable shear, tensional, and compressive strength.

4.2.2 Balsa Sheeting

Balsa sheeting will be used to construct the leading and trailing edge sheeting of the wings, tails, and control surfaces. It was selected for its very light, flexible, and smooth properties. It will help provide the desired aerodynamic shape and will be a surface onto which the UltraCote can adhere.

4.2.3 Aluminum

Aluminum will be the material of the wing and tail spars, the tail boom, and the landing gear. It was selected because it provides a high degree of shearing, tensional, and compressive strength (greater than that of wood) while still being relatively cheap and light compared to stronger alternatives such as steel.

It is worth noting, however, that—as seen in Sections 3 and 5—the selection of aluminum for the wing and tail spars leads to an incredibly high factor of safety. For this reason, one of the team’s possible future improvements for next semester would be to change the spars to basswood, as it would be much lighter.

4.2.4 UltraCote

UltraCote “is a high tech polyester airplane covering” [14]. It will be cut to size and used to coat the entire airplane, adhering it with a heating element such as an iron. It was chosen because it will provide the desire aerodynamic shape of the plane while adding nearly no weight. Additionally, it is designed to minimize skin friction drag.

4.2.5 Acrylonitrile Butadiene Styrene

Acrylonitrile Butadiene Styrene (ABS) is a plastic commonly used in 3D printers. It will be used to create the nose cone. It was selected because, through 3D printing, it can form complex shapes such as the nose-cone specific to the plane.

4.3 Manufacturing Processes

4.3.1 Laser-Cutting

Laser-cutting will be used to manufacture the wing and tail ribs and the fuselage panels. It was selected because it allows for the rapid, inexpensive production of components with complex geometry in two-dimensions such as ribs shaped like airfoils.

4.3.2 3D Printing

3D printing will be used to construct the nose cone. It was chosen because it allows for the construction of components with complex geometry in three-dimensions.

4.3.3 Bandsaw

Bandsaw cutting will be used to cut the spars and booms to size. It was selected because a bandsaw can cut aluminum.

4.3.4 Drill Press

Drill press drilling will be used to create the speed-holes in the tail boom as well as any holes needed to attach fasteners to metal. It was selected because a drill press can drill holes in metal.

4.3.5 Hot Iron

A hot iron will be used to adhere the UltraCote to the plane. This was chosen because a heating element is required to properly apply UltraCote.

5 Aircraft Performance Predictions

5.1 Lift and Drag Analysis

The lift and drag characteristics of the aircraft were analyzed using a combination of theoretical aerodynamic principles, XFLR5 simulations, and computational fluid dynamics (CFD) software. XFLR5 simulations were conducted under specific assumptions regarding flow and analysis methods. A viscous analysis was performed to account for boundary layer effects, and the ring vortex method (VLM2) was used for 3-D flow analysis, providing accurate predictions of lift and drag distributions. The simulations assumed steady, incompressible flow conditions, with a focus on laminar flow for simplicity. The results provide insight into the aircraft's aerodynamic efficiency and performance.

5.1.1 Lift Analysis

The lift coefficients were determined as follows:

- Zero-lift coefficient: $C_{L0} = 0.391$
- Lift curve slope ($C_{L,\alpha}$) = 4.584 rad^{-1}
- Maximum lift coefficient ($C_{L,max} = 1.48$)
- Maximum lift-to-drag ratio ($(C_L/C_D)_{max} = 9.8$)

The relationship between lift coefficient and angle of attack is illustrated in the graph below, showing a positive slope. Simulations were performed for both unloaded and loaded cases, with little to no visible difference observed in the lift curves between the two conditions.

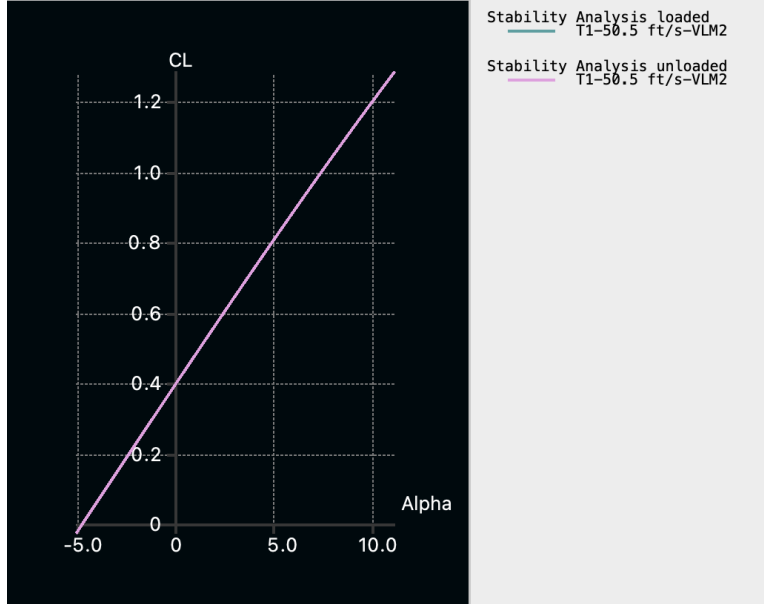


Figure 17: Lift analysis curves from XFLR5 for loaded and unloaded cases.

The lift distribution was obtained through XFLR5 analysis, which modeled the flow characteristics over the wings. The results show a more elliptical distribution compared to a purely rectangular wing, improving aerodynamic efficiency.

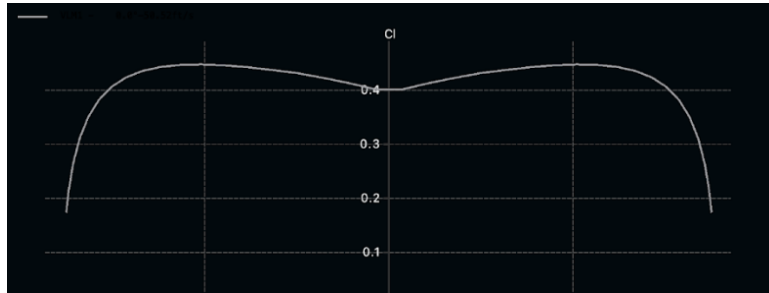


Figure 18: Lift Distribution from XFLR5 analysis.

5.1.2 Drag Analysis

The drag characteristics were broken down into components, and the total drag coefficient $C_{D0,total}$ was computed to be 0.07464. Contributions to drag were as follows:

- Vertical tail drag: $C_{D0,VT} = 0.00088$
- Horizontal tail drag: $C_{D0,HT} = 0.00572$
- Fuselage drag: $C_{D0,f} = 0.02537$

- Wing drag: $C_{D0,w} = 0.04267$

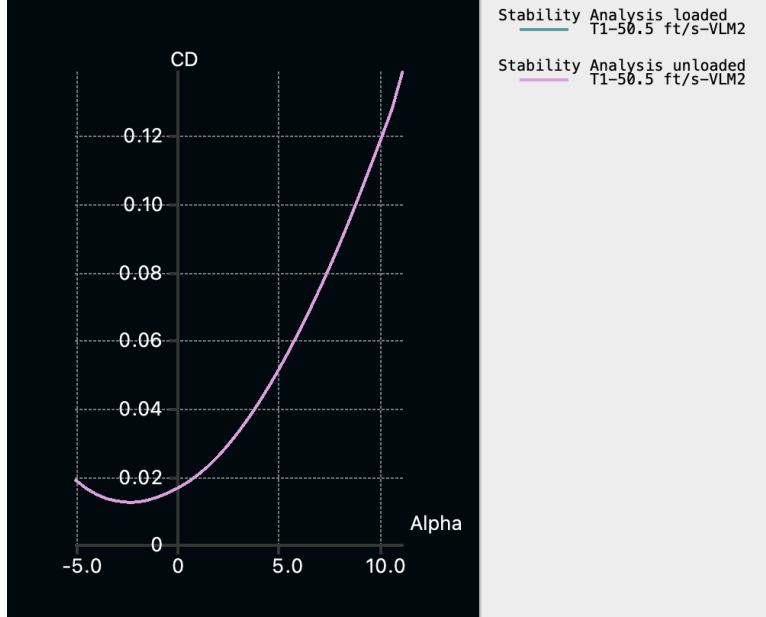


Figure 19: Drag analysis curves from XFLR5 for loaded and unloaded cases.

As mentioned in the Fuselage Design section, a fuselage drag analysis was conducted using SolidWorks Flow Simulation to determine the drag caused by the fuselage and landing gear. At a velocity of 17 m/s, the drag force was calculated to be 2.176 N, with a corresponding drag coefficient of $C_{D0} = 0.02537$. The simulation output highlights the velocity distribution around the fuselage, showing the areas of flow separation and drag contribution. Conducting this analysis provided insights into the aerodynamic impact of the fuselage and allowed the team to improve the design to minimize drag.

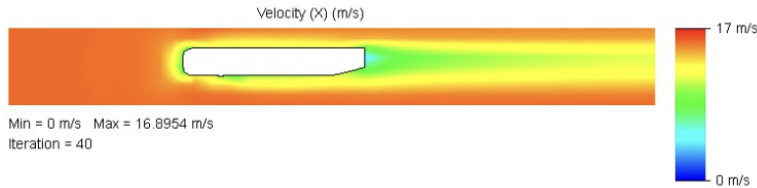


Figure 20: SolidWorks fuselage drag analysis results.

5.2 Stability Analysis

The stability analysis of the aircraft was performed using XFLR5, which provided both static and dynamic stability data. The analysis was carried out for unloaded and loaded cases to ensure stability under varying payload conditions. Results include directional static stability parameters and dynamic stability mode characteristics.

5.2.1 Static Stability Analysis

The static stability analysis focused on the aircraft's directional static stability, examining parameters such as the neutral point, center of gravity (CG) location, static margin, and trim angle of attack (α). The results for both unloaded and loaded cases are summarized below:

Table 12: Directional static stability parameters.

Parameter	Unloaded	Loaded
Neutral Point	6.792 in	6.805 in
Center of Gravity	5.667 in	5.809 in
Static Margin	0.106	0.081
Trim AoA	0.5°	2°
$C_{m,\alpha}$	-0.0089	-0.0067

The neutral point (NP) and center of gravity (CG) locations were determined through an iterative process using a combination of CAD geometry and XFLR5 analysis adjusting the payload and internal component placement looking at the C_m vs α curve. The negative slope of the C_m curve and the positive trim angle of attack indicates static stability for the aircraft.

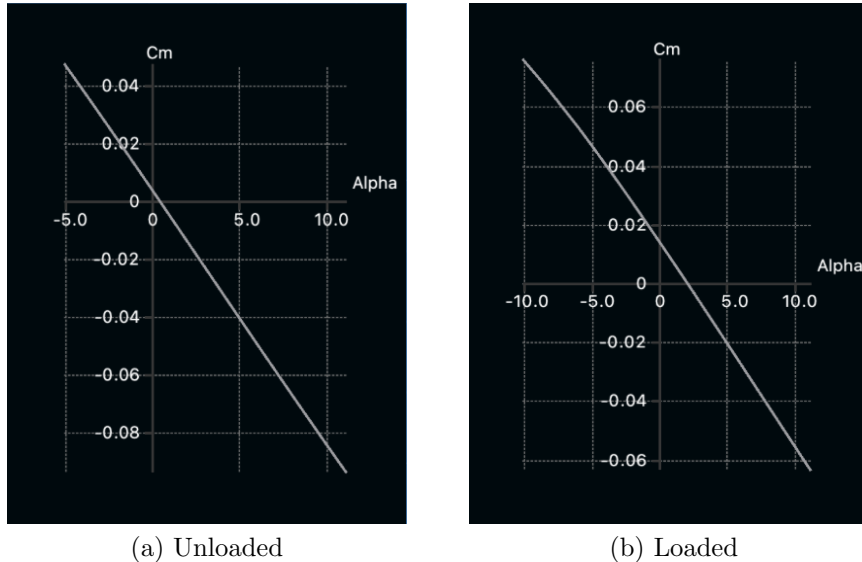


Figure 21: C_m vs α curves for both unloaded and loaded cases.

5.2.2 Dynamic Stability Analysis

Dynamic stability was assessed by analyzing the five primary longitudinal and lateral stability modes: Phugoid, Short Period, Roll, Spiral Divergence, and Dutch Roll. XFLR5 was used

to calculate the time constants, damping frequencies, and damping ratios for each mode. The results for unloaded and loaded cases are summarized in the tables below.

Table 13: Mode analysis results for the unloaded case.

Parameter	Phugoid	Short Period	Roll	Spiral Div.	Dutch Roll
Time to Double (non-oscillatory)	--	--	0.055 s	3.319 s	--
Damping Frequency (oscillatory)	0.097 Hz	0.792 Hz	--	--	0.816 Hz
Damping Ratio (oscillatory)	0.01	0.770	--	--	0.226

Table 14: Mode analysis results for the loaded case.

Parameter	Phugoid	Short Period	Roll	Spiral Div.	Dutch Roll
Time to Double(non-oscillatory)	--	--	0.049 s	3.405 s	--
Damping Frequency (oscillatory)	0.091 Hz	0.895 Hz	--	--	0.965 Hz
Damping Ratio (oscillatory)	0.001	0.732	--	--	0.223

From the analysis results, it can be observed that the short period mode is well-damped in both unloaded and loaded cases, ensuring good pitch stability. The roll mode shows fast time constants, indicating quick recovery in response to roll disturbances. The spiral divergence mode shows a slight divergence over time, which is a common characteristic in most aircraft designs, but it remains within acceptable limits. Lastly, the Dutch roll mode shows moderate damping, with slightly reduced values in the loaded case; however, it remains within stable margins.

5.3 Take-off Velocity

The loaded and unloaded takeoff velocities were calculated using data collected from XFLR5. During takeoff, the flaperon aerodynamic surfaces will be fully extended, as to maximize the lift output. By extending the aerodynamic surfaces, the increased lift will decrease the necessary takeoff distance. The takeoff wing configuration can be found in Figure 22,

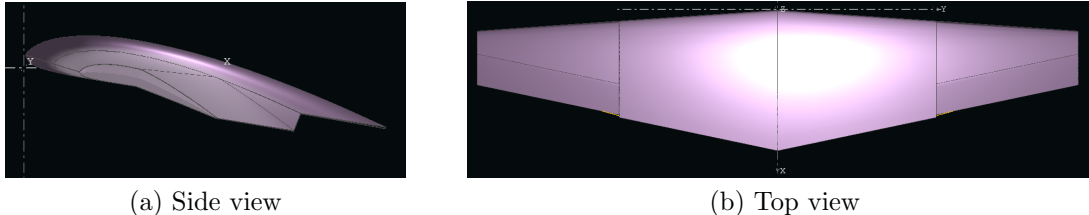


Figure 22: Wing takeoff configuration

The XFLR5 model in Figure 22 shows the constant area flaperons at their designated maximum extension of +12°. Using a fixed lift analysis in XFLR5, the loaded and unloaded lift coefficients were then tabulated in Table 15

Table 15: Take off lift coefficient.

Parameter	Unloaded	Loaded
$C_{L_{TO}}$	0.683	0.699

Finally using the results from the XFLR5 analysis, the loaded and unloaded takeoff speeds were calculated using the stall speed,

$$u_s = \sqrt{\frac{2W}{C_{L_{TO}}\rho S}}. \quad (16)$$

The stall speed is a good measure of the takeoff speed and does not need to be adjusted by a factor of 1.2 as it does for commercial flights because one goal of the project is to minimize the takeoff distance. Finally, the loaded and unloaded takeoff speeds are then tabulated in Table 16.

Table 16: Take off velocity.

Parameter	Unloaded	Loaded
Takeoff Velocity	7.662 ft/s	9.018 ft/s

5.4 Take-Off Distance

The unloaded and loaded take off distances were calculated for the plane design using the ground roll and rotation equations:

$$C_{LG} = 0.8C_{L,\max}, \quad (17)$$

$$AR_{\text{eff}} = AR\sqrt{\frac{b}{2H}}, \quad (18)$$

$$k_{\text{eff}} = \frac{1}{\pi e AR_{\text{eff}}}, \quad (19)$$

$$f_1 = g \left(\frac{T}{W_{TO}} - \mu \right), \quad (20)$$

$$f_2 = \frac{g\rho}{2 \left(\frac{W_{TO}}{S} \right)} \left(\mu C_{LG} - C_{D0} - k_{\text{eff}} C_{LG}^2 \right), \quad (21)$$

$$s_G = \frac{1}{2f_2} \ln \left(1 + \frac{f_2}{f_1} V_{TO}^2 \right), \quad (22)$$

$$s_R = 3[s] \cdot V_{TO}, \quad (23)$$

$$s_{TO} = s_G + s_R. \quad (24)$$

Using XFLR5 with the previously calculated plane geometry, it was determined that the unloaded take off distance was 24.2503 ft, and the loaded take off distance was 29.6228 ft.

5.5 Cruise Speed

The unloaded and loaded cruise speeds were calculated with the trim coefficients of lift determined in Section 5.1. The speeds were calculated via the equation

$$u_{cruise} = \sqrt{\frac{2W}{C_{Ltrim}\rho S}} \quad (25)$$

where W is the loaded or unloaded weight. The result of this analysis is summarized in Table 17.

Table 17: Cruise velocities.

Parameter	Unloaded	Loaded
Cruise Speed	54.04 ft/s	56.91 ft/s

5.6 Loading

The loading performance of the aircraft was derived using several assumption made to represent "worst-case-scenarios." First, the assumed load factor was the maximum load factor found in the wing design in Section 3. Second, to test the most severe case, it was assumed that the entire loading of the wing was placed solely on the main spar.

Using the cross-sectional dimensions of the chosen spar and the maximum moment and shear force from the plots in Figure 9, the maximum shear force and moment to which the wings would be subjected was calculated. This was done using the equations

$$\tau_{max} = \frac{\nu}{A} \quad (26)$$

and

$$\sigma_{max} = \frac{My}{I} \quad (27)$$

where τ_{max} is the maximum shear stress, σ_{max} is the maximum bending stress, ν is the maximum shear force, A is the cross-sectional area, M is the maximum moment, y is the maximum distance from the neutral axis and edge of the cross-section, and I is the second moment of area about the critical axis.

These values were calculated to be $\tau_{max} = 374.7$ psi and $\sigma_{max} = 2978$ psi. These values are far lower than the yield limits of aluminum, which are $\tau_y = 30000$ psi and $\sigma_y = 40000$ psi. As such, there is no concern in terms of the wing loading.

As a sanity check, however, an FEA analysis was also performed in SolidWorks. In the analysis, instead of using the calculated shear-moment diagrams, a direct load was applied, with magnitude determined by the maximum load factor and distribution determined by the XFLR5 lift distribution in Figure 6. Again, the wing was treated as a cantilever beam, and its stresses were measured. The set-up of this analysis can be found in Figure 23.

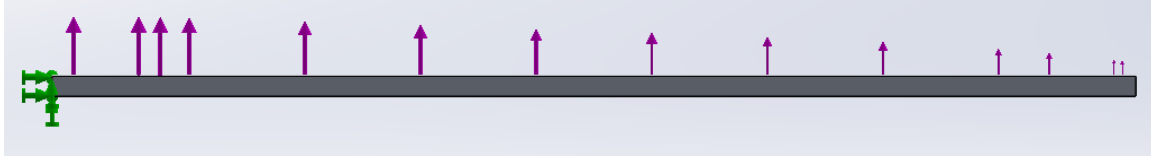


Figure 23: Loading of wing for FEA analysis.

The results of this FEA analysis were that the maximum shear and axial stresses experienced by the wing were $\tau_{max} = 240.9$ psi and $\sigma_{max} = 1568$ psi, respectively. These are even lower than the hand-calculation, likely because the hand calculated make assumptions such as free-shearing and no torsional-flexural coupling. Additionally, SolidWorks provided a Factor of Safety of 5.908 for the wing, which is significantly high.

5.7 Turning

The turning performance was found by using a MATLAB code which analyzed the characteristics of a RC plane under loaded and unloaded conditions. It was evaluated by finding the relationship between bank angles, turn rates, and turn radii. The script begins with defining the relevant parameters for the RC plane, including wing area, cruise speeds for both loaded and unloaded, weights, air density, and gravitational acceleration. These parameters are found in Table 7, 8, 9 and 19. The code then introduces the maximum and minimum load factors which are used to calculate the corresponding bank angles, turn rates, and turn radii. The maximum and minimum bank angles were determined by using the relationship between load factor and bank angle, where a higher load factor corresponds to steep turns. Using these load factors the maximum and minimum turn rates and turn radii were calculated. The code creates a range of bank angles from 0 to 60 degrees. Then for each bank angle the load factor is computed, from the load factor the turn rate and radii are derived using the formulas below:

$$R = \frac{V_\infty^2}{g\sqrt{n^2 - 1}} \quad (28)$$

$$\Psi = \frac{g\sqrt{n^2 - 1}}{v} \quad (29)$$

The results were then plotted, as shown in Figure 24. The first graph shows the turn radius as a function of bank angle, while the second graph shows the corresponding turn rate. Lastly the script displays the calculated maximum and minimum turn rates and radii, along with the corresponding bank angles for both loaded and unloaded cases. The visualizations and outputs provide clear insights into how the RC plane's turning performance changes with bank angle and weight. It highlights the trade-offs between tighter turns and higher turn rates, this analysis is crucial for understanding the maneuverability and flight limitations of the RC plane. The final results are located Table 18.

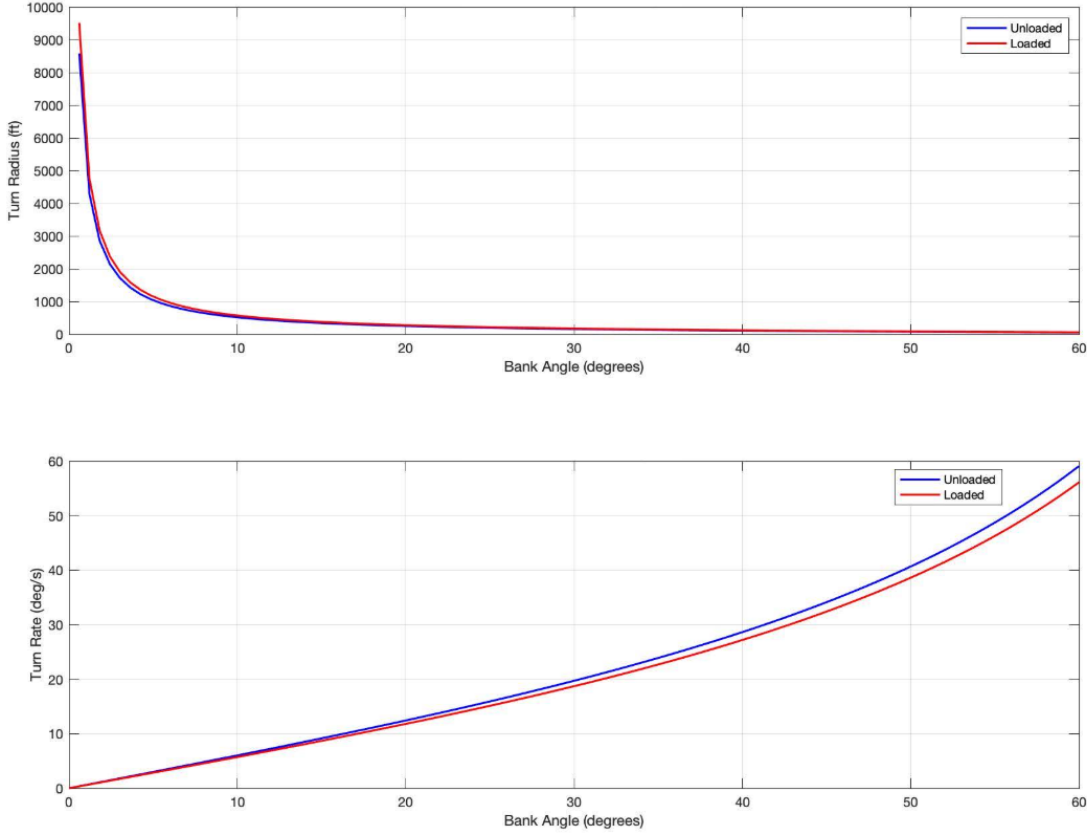


Figure 24: Turn radius and turn rate vs bank angle.

Table 18: Results of turning analysis.

Parameter	Loaded	Unloaded
Cruise Speed	56.9 ft/s	54.7 ft/s
Max Turn Rate	67.09 deg/s	62.99 deg/s
Min Turn Radius	49.15 ft	48.60 ft
Max Bank Angle	61.56 deg	64.23 deg

6 Aircraft Design Summary

6.1 Main Characteristics

The geometric characteristics of the wing are tabulated in Table 19. Those of the tails are tabulated in Table 20. Finally, those of the control surfaces are summarized in Table 21. Subsequently, detailed engineering drawings of the full plane design (with UltraCote not shown) are included.

Table 19: Summary of wing characteristics.

<u>Wing</u>	
Parameter	Value
Airfoil	N-22
Area, S	816.66 in ²
Span, b	70 in.
Aspect Ratio, AR	6.0
Root Chord, c_r	16.66 in.
Tip Chord, c_t	6.66 in.
Taper Ratio, λ	0.4
MAC, \bar{c}	12.38 in.
LE Sweep, Λ_{LE}	4.336°
$\bar{c}/4$ Sweep, $\Lambda_{\bar{c}/4}$	0°

Table 20: Summary of tail characteristics.

<u>Tails</u>	
Parameter	Value
Airfoils	NACA 0010
HT Area, S_{HT}	149.45 in ²
HT Span, b_{HT}	21.17 in.
HT Aspect Ratio, AR_{HT}	3.0
HT Chord, c_{HT}	7.05 in.
VT Area, S_{VT}	67.6 in ²
VT Span, b_{VT}	10.4 in.
VT Aspect Ratio, AR_{VT}	1.6
VT Chord, c_{VT}	6.5 in.

Table 21: Summary of control surface characteristics.

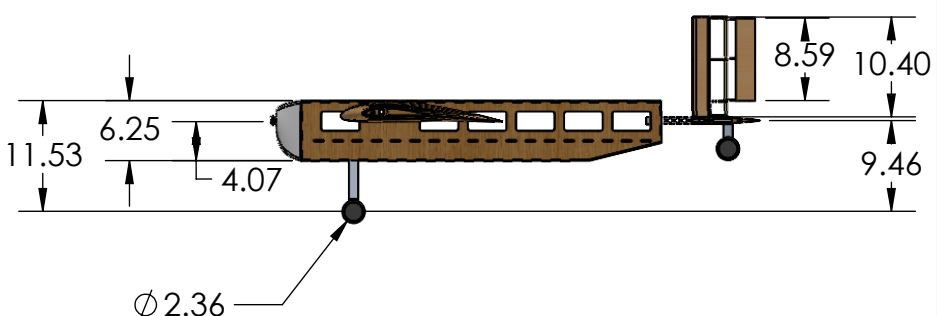
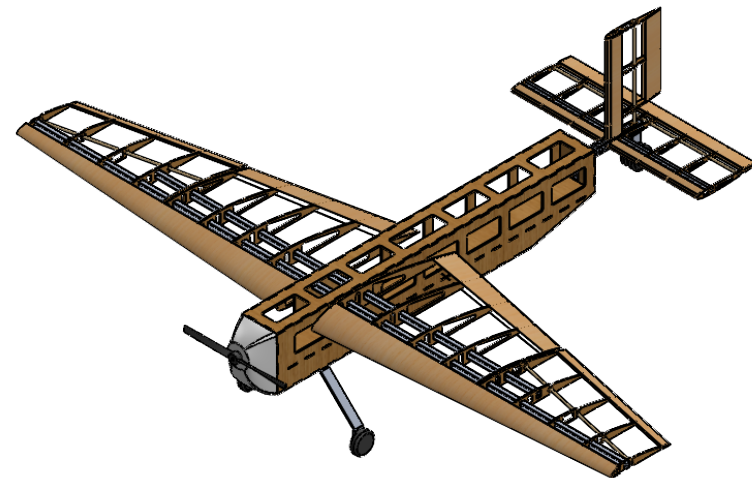
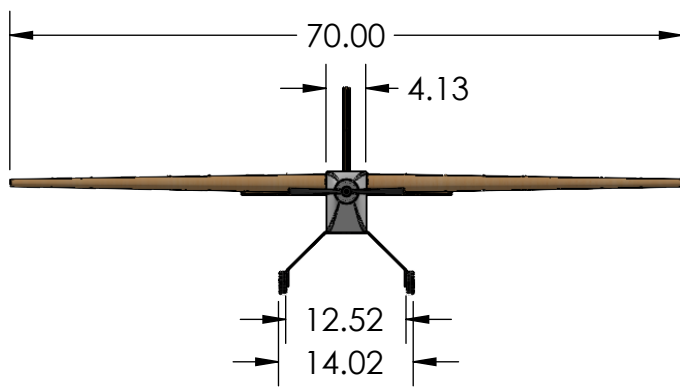
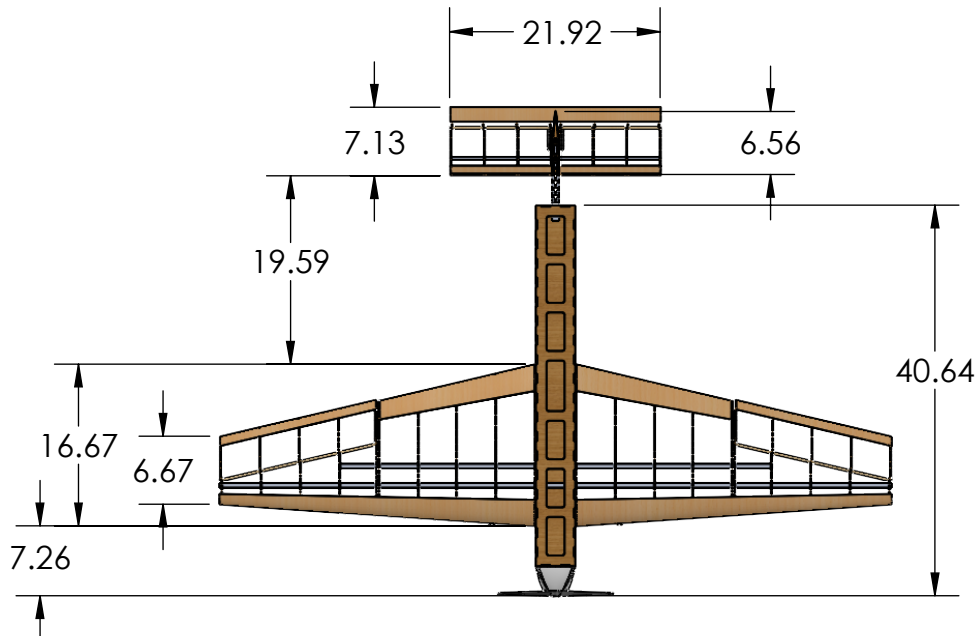
<u>Control Surface</u>	
Parameter	Value
Flaperon Area, S_f	148.95 in ²
Flaperon Span, b_f	33.1 in.
Flaperon Chord, c_f	4.5 in.
Elevator Area, S_e	44.835 in ²
Elevator Span, b_e	21.17 in.
Elevator Chord, c_e	2.118 in.
Rudder Area, S_r	31.772 in ²
Rudder Span, b_r	10.4 in.
Rudder Chord, c_r	3.055 in.

2

1

B

B



PROPRIETARY AND CONFIDENTIAL
THE INFORMATION CONTAINED IN THIS
DRAWING IS THE SOLE PROPERTY OF
NOTRE DAME ENGINEERING. ANY
REPRODUCTION IN PART OR AS A WHOLE
WITHOUT THE WRITTEN PERMISSION OF
NOTRE DAME ENGINEERING IS
PROHIBITED.

UNLESS OTHERWISE SPECIFIED:
DIMENSIONS ARE IN INCHES
TOLERANCES:
ANGULAR: MACH $\pm 1^\circ$
ONE PLACE DECIMAL ± 0.2
TWO PLACE DECIMAL ± 0.01
THREE PLACE DECIMAL ± 0.005

INTERPRET GEOMETRIC
TOLERANCING PER: ASME Y14.5

MATERIAL

NEXT ASSY

USED ON

FINISH

APPLICATION

DO NOT SCALE DRAWING

DRAWN NAME DATE

CHECKED

ENG APPR.

MFG APPR.

Q.A.

COMMENTS:

ND ENGINEERING

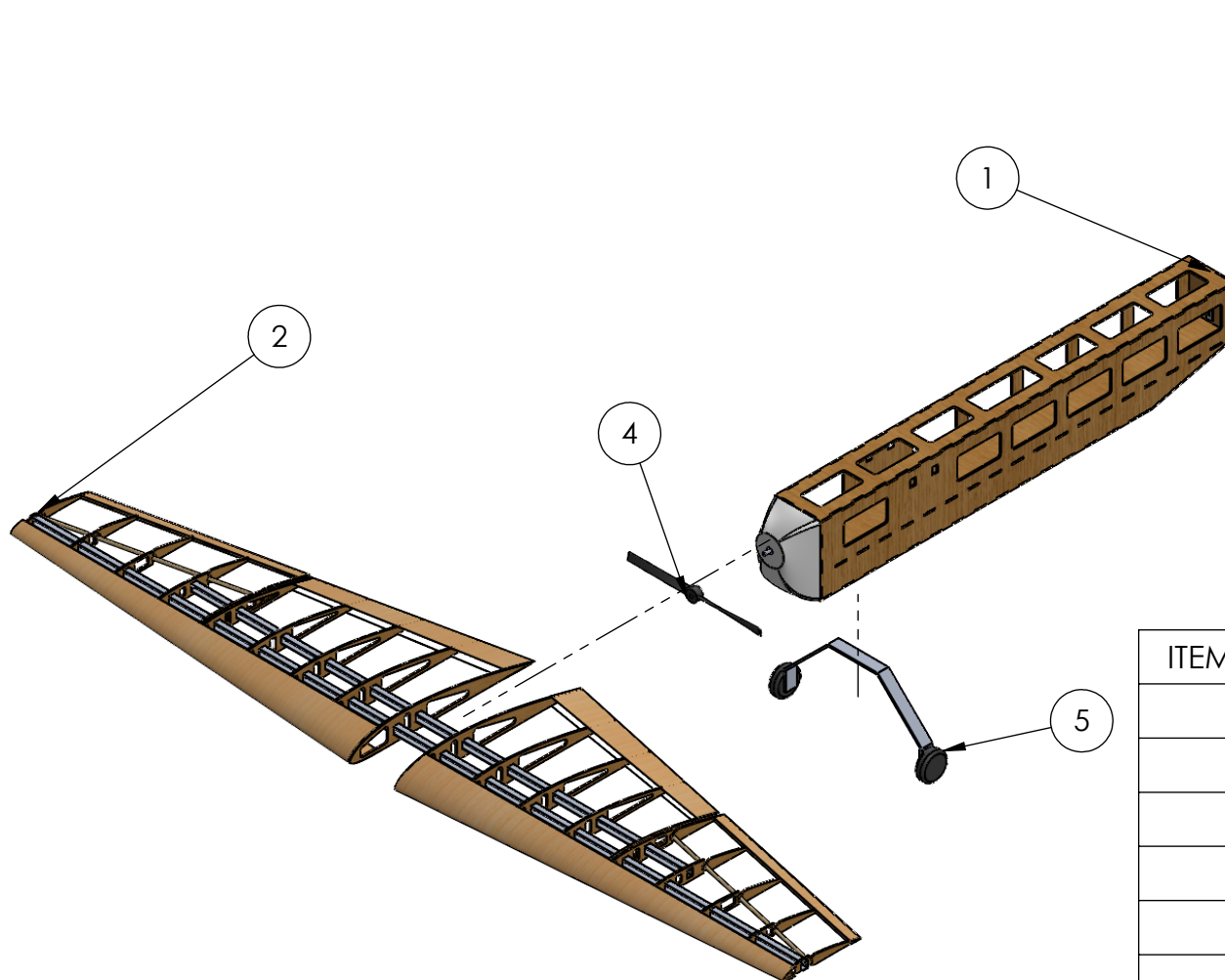
TITLE:

Plane Dimensioned

SIZE	DWG. NO.	REV
A	PLANE-1	
SCALE: 1:24		SHEET 1 OF 1

2

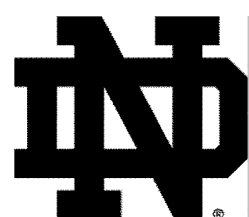
1



1

3

6



PROPRIETARY AND CONFIDENTIAL
THE INFORMATION CONTAINED IN THIS DRAWING IS THE SOLE PROPERTY OF NOTRE DAME ENGINEERING. ANY REPRODUCTION IN PART OR AS A WHOLE WITHOUT THE WRITTEN PERMISSION OF NOTRE DAME ENGINEERING IS PROHIBITED.

UNLESS OTHERWISE SPECIFIED:
DIMENSIONS ARE IN INCHES
TOLERANCES:
ANGULAR: MACH $\pm 1^\circ$
ONE PLACE DECIMAL ± 0.2
TWO PLACE DECIMAL ± 0.01
THREE PLACE DECIMAL ± 0.005

INTERPRET GEOMETRIC
TOLERANCING PER: ASME Y14.5

MATERIAL

NEXT ASSY USED ON

FINISH

APPLICATION

DO NOT SCALE DRAWING

ITEM NO.	PART NUMBER	QTY.
1	FuselageAssembly	1
2	wingsAssem	1
3	tailAssem	1
4	propeller	1
5	Landing_gear	1
6	Landing_gear2	1

NAME DATE

ND ENGINEERING

TITLE:

Plane Exploded

SIZE	DWG. NO.	REV
A	PLANE-2	
SCALE: 1:32		SHEET 1 OF 1

Furthermore, a summary of the plane's performance characteristics are tabulated in Table 22, and a summary of its loading characteristics are included in Table 23.

Table 22: Summary of performance characteristics.

<u>Performance</u>		
Parameter	Unloaded	Loaded
TO Speed	7.662 ft/s	9.018 ft/s
Cruise Speed	54.04 ft/s	56.91 ft/s
TO Distance	24.25 ft	29.62 ft
Min. Turn Radius	49.15 ft	48.60 ft
Max. Bank Angle	61.56 deg	64.23 deg
Max. Turn Rate	63.04 deg/s	67.15 deg/s

Table 23: Summary of loading characteristics.

<u>Weights and Loading</u>		
Parameter	Unloaded	Loaded
Weight	8.744 lb	12.279 lb
Wing Loading	0.0104 psi	0.0147 psi
Max Load Factor	2.1	2.3
Max Gust Load Factor	5.95	5.70

6.2 Uniqueness

The RC aircraft presented incorporates several innovative design features that enhance performance, efficiency, and stability. There are several aspects that distinguish this aircraft from a conventional RC planes: First factor of uniqueness is the optimized nose cone. The nose cone was carefully designed to minimize drag and improve aerodynamic efficiency. This optimization ensures smoother airflow around the fuselage which is important for extending flight duration and reducing drag. Another unique feature of the RC plane is the tapered wings. The wings feature a tapered design that lowers drag and improves maneuverability. The unswept quarter-chord configuration ensures stable flight dynamics while maintaining simplicity in construction. These characteristics contribute to a balance of agility and efficiency, which is essential for RC aircraft.

The boom tail configuration is another unique feature of the RC aircraft. By using the boomtail the design achieves a significant weight reduction and enhanced stability. A lighter structure allows for increased payload capacity or extended flight time, while improved stability ensures predictable and controlled responses during maneuvers. Lastly, looking into inputting a stability augmentation system would also increase the uniqueness score. This would further enhance flight stability and control. The system mitigates perturbations and

Senior Design Final Report

simplifies pilot inputs, which is especially beneficial for RC planes that may be subject to unpredictable wind conditions or piloting challenges.

Each of these features demonstrate a unique approach to optimize the aerodynamics, weight, and control systems of the aircraft. In theory this should result in a highly efficient and stable design tailored for RC flight performance.

References

- [1] Corke, T. C., *Design of Aircraft*, Pearson Education, 2002.
- [2] JoyPlanes, “Selection of Airfoil — Model Airplanes,” online, 2022, accessed November 13, 2024.
- [3] FliteTest, “Which Airfoil Should I Use?” online, 2018, accessed November 13, 2024.
- [4] Airfield Models, “About Airfoils for Flying Model Aircraft,” online, 2021, accessed November 13, 2024.
- [5] RC Groups, “Which airfoil to use,” online, 2014, accessed November 13, 2024.
- [6] XFLR5, “XFLR5: Analysis of Airfoils, Wings, and Aircrafts, Version 6.61,” online software, 2024, accessed December 9, 2024.
- [7] One Monroe Aerospace, “The Pros and Cons of a T-Tail Empennage,” online, 2023, accessed November 13, 2024.
- [8] Megson, T., *Aircraft Structures for Engineering Students*, Butterworth-Heinemann, 2022.
- [9] RC Groups, “How much load can rc planes take?” online, 2009, accessed December 9, 2024.
- [10] MatWeb, “Plywood Material Data Sheet,” online, 1999, accessed December 6, 2024.
- [11] Nelson, R. C., *Flight Stability and Automatic Control*, McGraw-Hill, 1998.
- [12] Home Depot, “1/4 in. x 48 in. Round Dowel,” online, 2024, accessed December 4, 2024.
- [13] Home Depot, “Everbilt Square Tube,” online, 2024, accessed December 5, 2024.
- [14] Horizon Hobby, “UltraCote,” online, 2024, accessed December 13, 2024.